Hindawi
Mathematical Problems in Engineering
Volume 2019, Article ID 4191924, 16 pages
https://doi.org/10.1155/2019/4191924

Research Article

Effective Hybrid Algorithm of Taguchi Method, FEM, RSM, and Teaching Learning-Based Optimization for Multiobjective Optimization Design of a Compliant Rotary Positioning Stage for Nanoindentation Tester

Minh Phung Dang,[1] Thanh-Phong Dao ,[2,3] Ngoc Le Chau,[4] and Hieu Giang Le[1]

[1] *Faculty of Mechanical Engineering, Ho Chi Minh City University of Technology and Education, Ho Chi Minh City, Vietnam*
[2] *Division of Computational Mechatronics, Institute for Computational Science, Ton Duc Thang University, Ho Chi Minh City, Vietnam*
[3] *Faculty of Electrical & Electronics Engineering, Ton Duc Thang University, Ho Chi Minh City, Vietnam*
[4] *Faculty of Mechanical Engineering, Industrial University of Ho Chi Minh City, Ho Chi Minh City, Vietnam*

Correspondence should be addressed to Thanh-Phong Dao; daothanhphong@tdtu.edu.vn

Received 26 October 2018; Revised 13 December 2018; Accepted 16 December 2018; Published 15 January 2019

Academic Editor: Thomas Hanne

This paper proposes an effective hybrid optimization algorithm for multiobjective optimization design of a compliant rotary positioning stage for indentation tester. The stage is created with respect to the Beetle's profile. To meet practical demands of the stage, the geometric parameters are optimized so as to find the best performances. In the present work, the Taguchi method is employed to lay out the number of numerical experiments. Subsequently, the finite element method is built to retrieve the numerical data. The mathematical models are then established based on the response surface method. Before conducting the optimization implementation, the weight factor of each response is calculated exactly. Based on the well-established models, the multiple performances are simultaneously optimized utilizing the teaching learning-based optimization. The results found that the weight factors of safety factor and displacement are 0.5995 (59.95%) and 0.4005 (40.05%), respectively. The results revealed that the optimal safety factor is about 1.558 and the optimal displacement is 2.096 mm. The validations are in good agreement with the predicted results. Sensitivity analysis is carried out to identify the effects of variables on the responses. Using the Wilcoxon's rank signed test and Friedman test, the effectiveness of the proposed hybrid approach is better than that of other evolutionary algorithms. It ensures a good effectiveness to solve a complex multiobjective optimization problem.

1. Introduction

Nanoindentation tester is designed to provide low loads with depth measurements in the nanometer scale for the measurement of hardness, elastic modulus, and creep. The system can be used to characterize organic, inorganic, hard, and soft materials. With the unique top surface referencing technique, an indentation measurement can be made in less than 3 minutes without waiting for thermal stabilization. Hence, the positioning process has to be with high accuracy. Materials can be tested, including hard and soft types from tissue, biological cell, nanomaterial, optics, material science, semiconductor, biomechanics, microelectromechanical systems, and electronics [1–3]. During the indentation process, the multiple microscopes are used to record the image of sample before and after indenting test to characterize the curve of displacement versus load while a material sample is brought in front of microscope. In order to achieve a good image quality, a precise positioning stage is essential. It means that a positioning stage is an important mechanism for the nanoindentation tester. In commercialization, the current positioning stage is difficult to allow a high position precision because of the unfavorable influences of backlash, friction, and wear existing in rigid kinematic joints.

To overcome the disadvantages of traditional technologies, the compliant micropositioning rotary stage is proposed to enhance resolution because of their essential merits such as no wear, no backlash, free friction, light weight, low cost, no lubricant, monolithic structure, high precision, and compact structure [4–8]. Similar to various applications, the indentation system also needs large strokes with a high safety factor for positioning tasks. This is strongly dependent on the proposed stage.

A few recent years, researchers centered on development for large working platforms [9, 10]. Zhu et al. designed an amplifier combining the Scott-Russell mechanism and half-bridge mechanism for XY nanopositioning stage [11]. Kim et al. used a double amplification mechanism for 3-DOFs flexure-based positioning system [12]. Besides, compliant rotary stage with large angle was proposed [13]. However, a positioning stage for nanoindentation tester, which is transferring a translation to rotation, lacks interest.

In order to meet the practical requirements of advanced material sciences, the capability of a large positioning space and long working life of the proposed stage should be enhanced further. Generally, a lever amplifier or a bridge one is widely utilized to improve the working travel of the platform. In this study, in order to obtain a good stroke, the four-lever amplifier is monolithically integrated in the stage. Even though the amplifier can improve the working travel, it is still limited. Therefore, a multiple objective optimization design is conducted in this study so as to enhance overall the static performances, simultaneously. For structural optimization, topology, size, or shape optimization is used. Topology permits the connectivity of the domain while the size optimization denotes design [10, 17–20]. Shape optimization gives a suitable configuration. In the present work, the size optimization is chosen while the shape configuration of proposed stage is designed based on the designer's experiences. Due to the fact that mathematical models for the stage are relatively complicated, an optimization solution may not be accurate. Common evolutionary algorithms often require initially controllable parameters, for instance, genetic algorithm [21, 22], partial swarm optimization [23–26], and differential evolution algorithm [27]. In contrast, the teaching learning-based optimization algorithm (TLBO) [28–31] can optimize rapidly multicriteria and minimize calculating effort with less controllable parameters. Meanwhile, the application of the TLBO algorithm for the rotary positioning stage has not been interested yet. To improve the convergence speed and achieve more accuracy, a combination of the Taguchi method (TM), finite element method (FEM), response surface method (RSM), and teaching learning-based optimization (TLBO) was proposed to solve multiobjective optimization based on advantages of these methods. The TM utilizes the most suitable orthogonal arrays based on the combination of factors to build the number of experiments [32, 33]. Such data-driven multiple optimization approach can limit the undesired errors from the analytical methods. Individually, the FEM has been widely used in various engineering fields [34–36]. In this research, the FEM is utilized to retrieve the two quality responses of the stage based on the number of experiments. Moreover, the RSM [37] can establish the regression models to find relationship between the parameters and quality responses before implementing an optimization problem by the TLBO. An integration of hybrid algorithm has not been investigated for the stage yet.

As a result, the proposed hybrid algorithm is developed to solve multiobjective optimization design in the present work, simultaneously. As known, multiple objectives often conflict each other. In order to seek a balance among them, a weight factor (WF) should be assigned for each response. The WF is almost determined relying on the priority of responses or designer's experiences. Unlike previous studies, prior to an optimization, mathematical models are built to determine exactly the WF.

The main goal of this paper is to develop a new hybrid optimization approach for solving the multiobjective optimization design of compliant rotary positioning stage in terms of good static characteristics in order to balance conflicted performances of the two quality responses and reduce the time computing with less controllable parameters. The sensitivity analysis is then analyzed based on the statistical method. The data are collected using an integration of TM and FEM. The equations are formed by RSM. The WF is computed, and the optimization solutions are sought through TLBO. Next, the verifications are conducted to validate the predicted results. At last, a few statistical analyses are carried out to compare the hybrid approach with other methods.

2. Design of Compliant Rotary Positioning Stage

2.1. Kinetic Structure. A lot of compliant micropositioning stages from one degree of freedom (DOF) [14], 2 DOFs [15], and 3 DOFs [16] were illustrated in Figures 1(a)–1(c), respectively. However, a compliant rotary positioning stage (CRPS) for indentation device has been less researched. In this study, a linear motion would be transferred to a rotation to locate the sample material for testing by indenter and monitoring by microscope before and after indentation. If a rotary platform was directly designed by only pure rotation, a further controller is complicated. Meanwhile, from the translation to rotation, the proposed stage could be controlled easily by solving the linear end. Summarily, the operation principle of the proposed CRPS was moved from a linear movement to rotary motion, as given in Figure 1(d).

2.2. Hybrid Displacement Amplifier. The lever mechanism is still a useful structure to amplify the load or the displacement. Structure of the lever includes a beam or rigid rod placed on a fixed hinge, or fulcrum, as illustrated in Figure 2. Point O is considered a rotation center of the lever, A is the input end, and B is the output end. The operation principle of lever mechanism is described as follows: when locating a vertical displacement Δl_1 on the input point A, the lever will rotate an γ angle relative to the z-axis. As a result, the point B moves to B' and the output displacement Δl_2 can gain in the vertical direction (y-axis). Firstly, one lever mechanism can be used to amplify output displacement, as depicted in Figure 3(a) (Case 1). However, this mechanism creates easily a large parasitic motion. Moreover, in order to amplify more large output

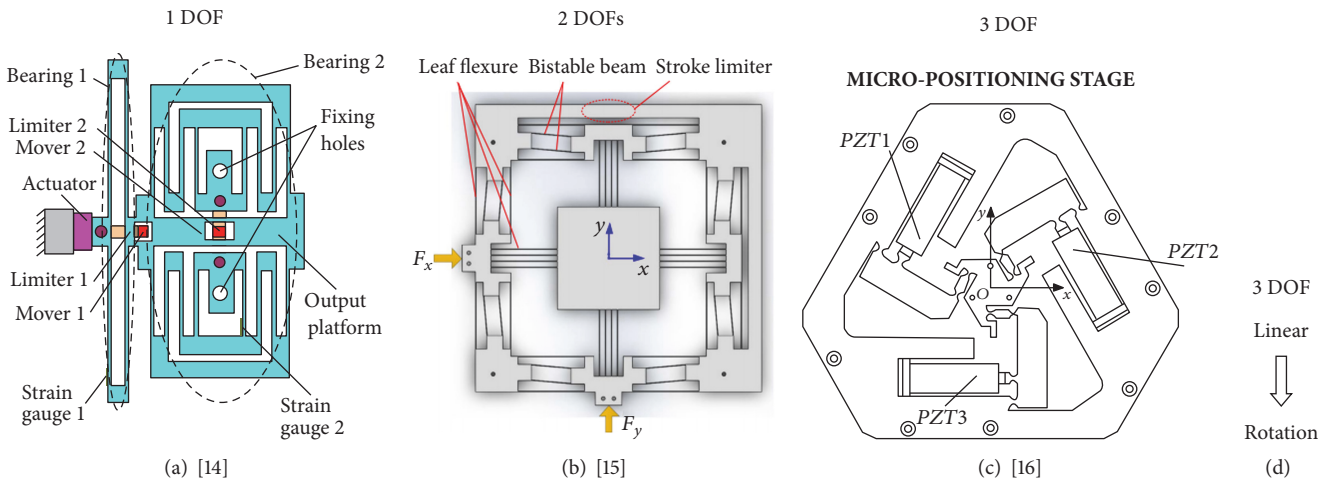

Figure 1: Various micropositioning stages: (a) 1 DOF micropositioning stage, (b) 2 DOF micropositioning stage, and (c) 3 DOF micropositioning stage.

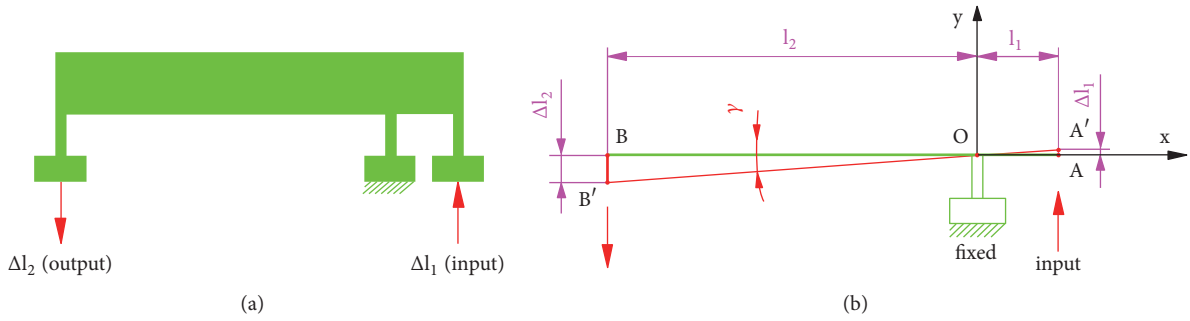

Figure 2: Schematics of (a) the operation principle of lever mechanism and (b) analysis of amplification ratio.

displacement and generate linear motion based on symmetric structure, four-lever displacement amplifier is proposed so as to gain more large displacement and linear displacement, as depicted in Figure 3(b) (Case 2). Thanks to the structural characteristics of the amplifier, the amplification ratio can be approximately achieved by

$$r_{lever} = \frac{\Delta l_2}{\Delta l_1} = \frac{l_2}{l_1}. \quad (1)$$

The equation of multilever displacement amplifier is assumed as follows:

$$r_{lever} = N \times \frac{l_2}{l_1}. \quad (2)$$

A finite element analysis (FEA) in ANSYS software was used to model and compare the amplification ratio between case 1 and case 2. Boundary conditions for both cases were given in Figures 3(a) and 3(b). The value of input displacement was assigned within the range from 0.1 mm to 0.24 mm. The Y_{old} and Y_{new} representing the output displacement of case 1 and case 2 along the Y-axis, respectively, were retrieved. The amplification ratios for the case 1 and case 2 were computed as R_{old} and R_{new}, respectively, in Tables 1 and 2. An improvement of the amplification ratio is about 221.6 %, as given in Table 3 and Figure 4.

Table 1: Amplification ratio for case 1.

Input (mm)	Y_{old} (mm)	R_{old}
0.1	0.443	4.43
0.12	0.532	4.43
0.14	0.620	4.43
0.16	0.709	4.43
0.18	0.797	4.43
0.2	0.886	4.43
0.22	0.975	4.43
0.24	1.063	4.43

3. Compliant Rotary Positioning Stage

The operating principle of CRPS was based on the elastic deformation of the material. The CRPS was used for locating the sample during nanoindentation testing. A basic application for nanoindentation tester was proposed in Figure 5. The material Al 7075 was selected for the proposed CRPS because of its high yield strength of 503 MPa, Young's modulus of E = 71700 MPa, a light density of 2770 kg/m^3, and Poisson's ratio of 0.33. Specification of rotary stage assumed that input displacement was 0.19 mm. The CRPS was proposed,

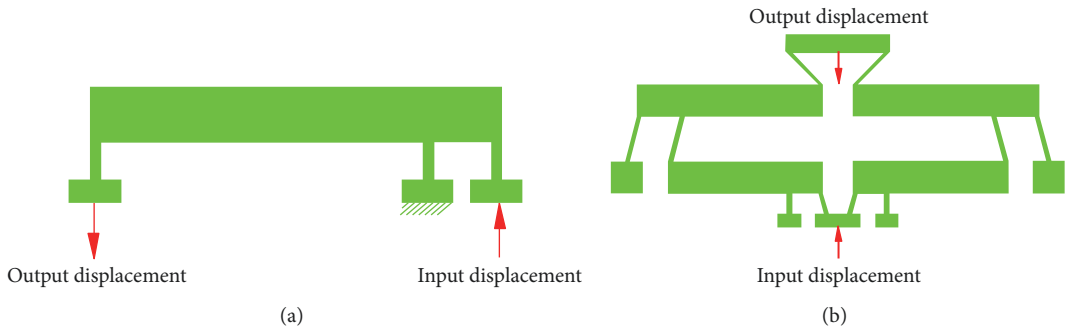

Figure 3: Model of lever amplifiers: (a) case 1: one lever mechanism and (b) case 2: four-lever mechanism.

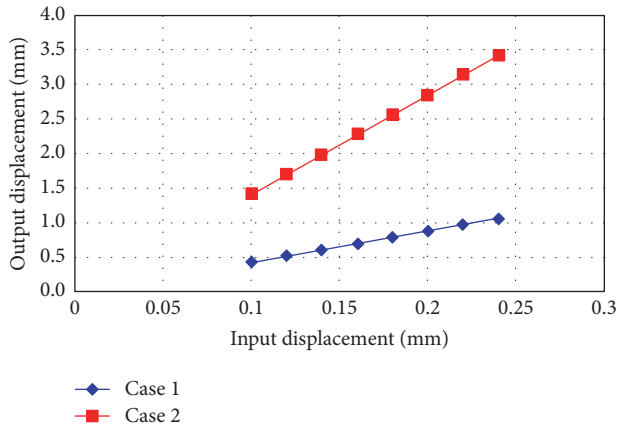

Figure 4: Input displacement vs. output displacement for case 1 and case 2.

Table 2: Amplification ratio for case 2.

Input (mm)	Y_{new} (mm)	R_{new}
0.1	1.425	14.25
0.12	1.710	14.25
0.14	1.995	14.25
0.16	2.280	14.25
0.18	2.564	14.25
0.2	2.849	14.25
0.22	3.134	14.25
0.24	3.419	14.25

as seen in Figure 6. It was designed based on the Beetle's profile to get a good compliance. It consisted of elements as follows: (i) sixteen fixed holes were utilized to locate the platform on an unvibration table and (ii) a piezoelectric actuator (PZT) (locating at the input displacement position) was used to create the input displacement for the stage by connecting directly with the beetle-like structure and rotary mechanism. The total dimension of the model was approximately 280 mm×376 mm×6 mm. The proposed rotary stage was designed to create a linear displacement, and a large rotary angle for indentation testing would be increased accordingly. Geometrical parameters of the proposed rotary stage were given in Figure 7 and Table 4. Among the geometrical parameters, factors A, B, C, and D were selected as the design variables because they had a large effect on the responses. Meanwhile, the others were chosen as constant.

4. Formulation of Multiobjective Optimization Problem

In this study, the CRPS needs to fulfill responses such as the following. (i): Safety factor (F_1) should be as large as possible to increase the long fatigue life and avoid plastic failure of the material. (ii) Large y-axis displacement (F_2) should be large to expand working travel. The optimization problem for the rotary stage can be summarized as follows.

Find the design variables: $\mathbf{X} = [A, B, C, D]$

Maximize safety factor as

$$F_1(A, B, C, D) \geq 1.5, \tag{3}$$

Maximize the displacement (F_2) as

$$F_2(A, B, C, D) \geq 1.55\,\text{mm}, \tag{4}$$

Subject to constraints

$$\begin{aligned} 51\,\text{mm} \leq A \leq 53\,\text{mm}, \\ 1\,\text{mm} \leq B \leq 1.2\,\text{mm}, \\ 0.5\,\text{mm} \leq C \leq 0.7\,\text{mm}, \\ 0.5\,\text{mm} \leq D \leq 0.7\,\text{mm}, \end{aligned} \tag{5}$$

where F_1 and F_2 are the objective responses. A, B, C, and D are the length of first lever, thickness of flexure hinge (lever amplifier), thickness of flexure hinge (beetle's leg mechanism), and thickness of flexure hinge (rotary mechanism), respectively.

5. Methodology

Regarding the multiple response optimization problem, a hybrid approach was proposed in the present work. In this study, a large displacement is expected to expand a range of working travel and meet a wide application and a safety factor is desired to enhance a fatigue life for the structure.

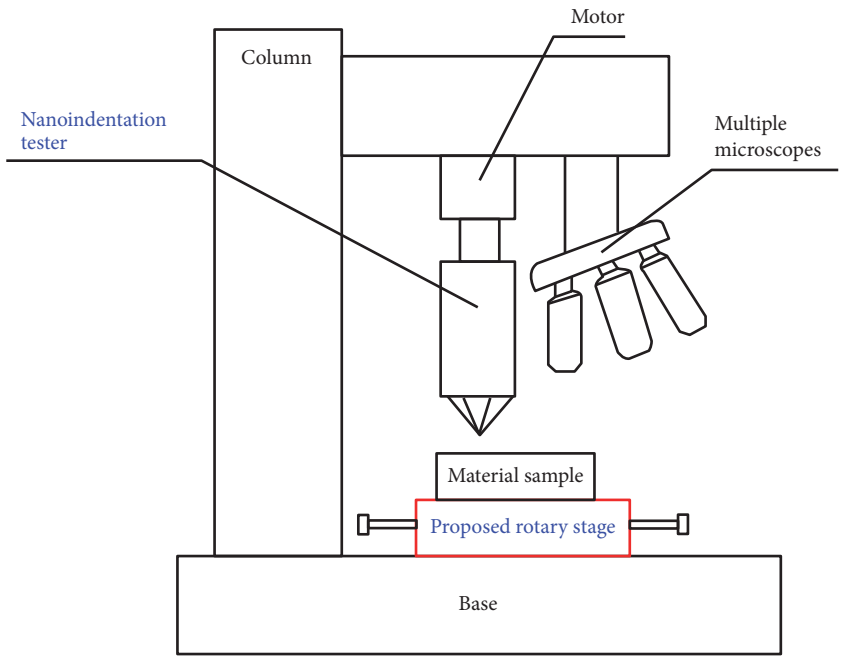

Figure 5: Nanoindentation testing system.

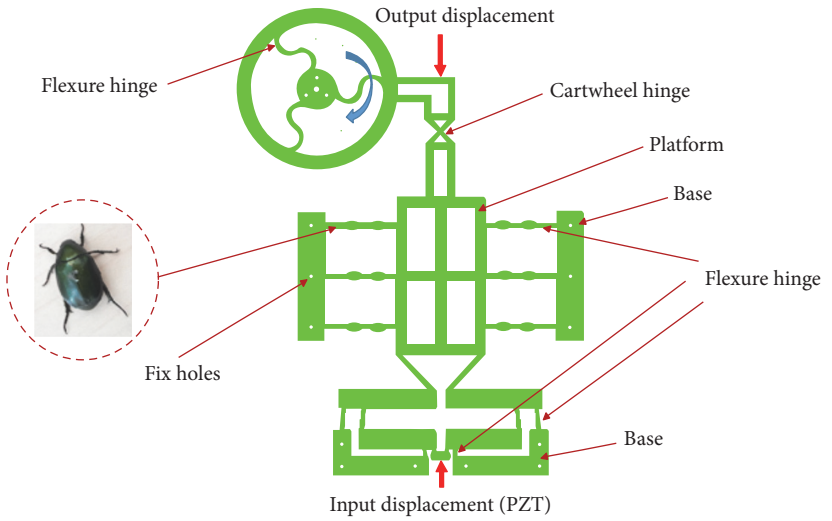

Figure 6: Model of beetle-inspired stage.

Table 3: Comparison between the amplification ratios of case 1 and case 2.

Input (mm)	R_{old}	R_{new}	Improvement (%)
0.1	4.43	14.25	221.6
0.12	4.43	14.25	221.6
0.14	4.43	14.25	221.6
0.16	4.43	14.25	221.6
0.18	4.43	14.25	221.6
0.2	4.43	14.25	221.6
0.22	4.43	14.25	221.6
0.24	4.43	14.25	221.6

Table 4: Geometrical parameters of the rotary stage (unit: mm).

Parameters	Value	Parameters	Value	Parameters	Value
a	6.84	m	222	x	30
b	20	n	230	y	280
c	8	o	70	z	376
d	30	p	30	A	$51 \le A \le 53$
e	76	q	70	B	$1 \le B \le 1.2$
f	6	r	65	C	$0.5 \le C \le 0.7$
g	5	t	10	D	$0.5 \le D \le 0.7$
h	102				

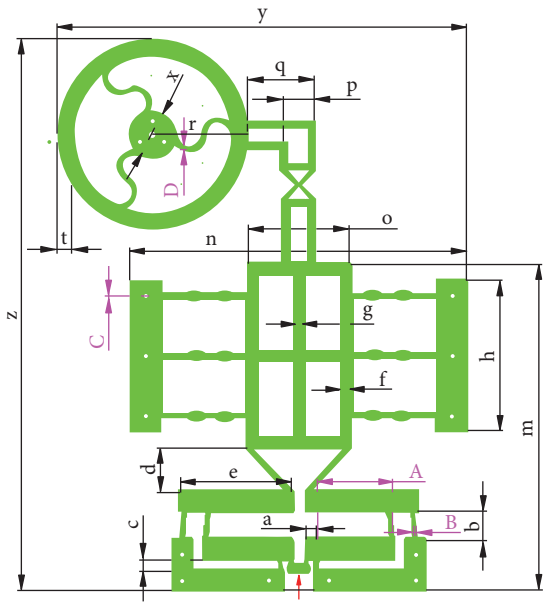

Figure 7: Design parameters for the compliant rotary positioning stage.

However, a large displacement is always conflicted with a high safety factor. A hybrid approach of TM, FEM, RSM, and TLBO was developed so as to solve a trade-off between the displacement and safety factor. The hybrid approach included the following main steps. (1) The TM was utilized to establish the number of experiments. (2) The FEM was utilized to build 3D model and retrieve the displacement and safety factor. (3) The RSM was used to establish the number of experiments. (4) Finally, the optimal solutions were determined by using the TLBO algorithm. A flowchart of the proposed hybrid approach was illustrated in Figure 8. It consisted of several phases and substeps as follows.

Phase 1 (computer-aided engineering design). Along with efficient support from a high performance computer, thousands of computational analyses per second can be done well. In order to optimize the CRPS, a CAED was conducted by the following steps.

Step 1 (define optimal problem). The CRPS was designed to serve as a positioning platform in an indentation system. A PZT was utilized to give the input motion for the CRPS but PZT's travel was limited. Therefore, the purpose of this study is to optimize geometric parameters of the stage. The first quality objective is to maximize safety factor and the second objective is to maximize the displacement. Multiobjective optimization problem for the CRPS was conducted to enhance both quality performances.

Step 2 (mechanical structure). A few draft models were designed based on beetle animal to make a good compliant structure and to describe the initial operations of the stage. An eventual model was selected.

Step 3 (design variables and quality responses). The length of first lever A, thickness of flexure hinge B, thickness of flexure hinge C, and thickness of flexure hinge D were determined as design variables for achieving the best quality objectives. The reason was that these parameters affect significantly the performances of the CRPS. These variables can be seen as Figure 7. To meet the practical requirements of customers, a large working stroke and a high safety factor can be fulfilled by optimizing simultaneously.

Step 4 (build 3D-FEM model). A 3D-FEM model was designed so as to serve for computational analysis, and the quality characteristics were retrieved.

Step 5 (evaluate initial quality characteristics). The 3D-FEM model was analyzed. If the stage's specifications were not satisfied according to the designer's requirements, the process would return to Step 2. Otherwise, it would move to Phase 2.

Phase 2 (response surface method and regression model). In order to conduct optimal process, a number of experiments were generated and numerical data were collected. Later on, the regression models were established to map design variables and the quality responses.

Step 6 (design of experiment). Firstly, the TM was used to determine an orthogonal array to establish the number of numerical experiments because it allowed a small number of experiments. In addition, analysis of variance (ANOVA) was employed to find the significant contribution of design variables.

Step 7 (generate data). The numerical experimentations were retrieved based on a hybrid integration of FEM and RSM, using a 3D-FEM model which was designed in Step 4.

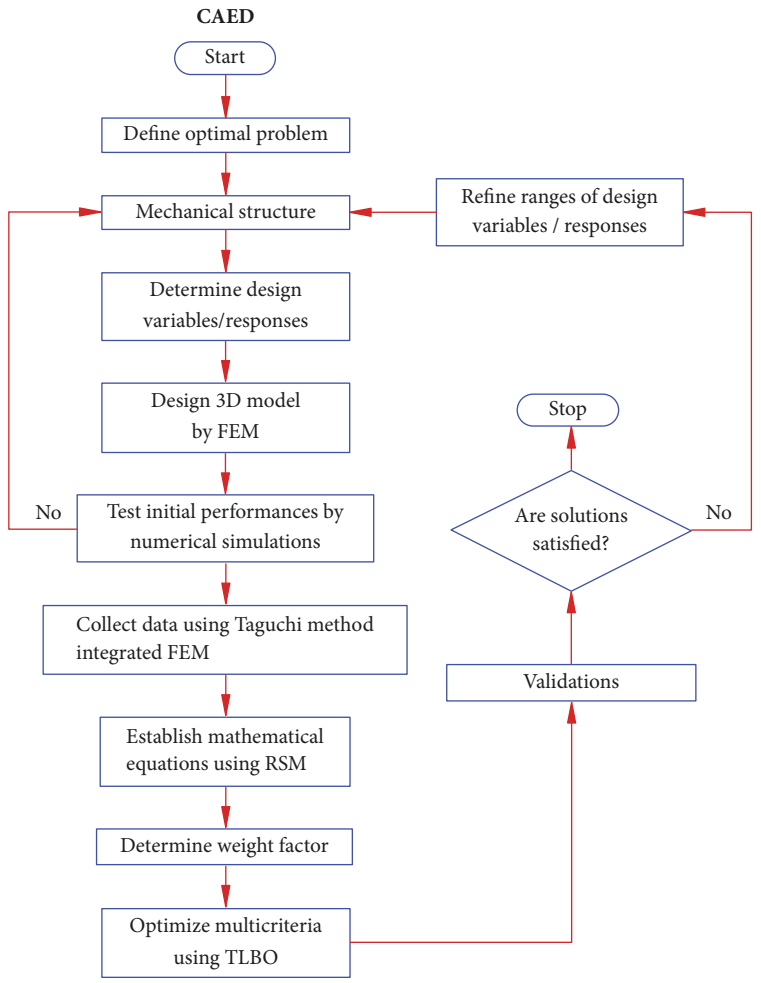

Figure 8: Flowchart of multiobjective optimization approach.

Subsequently, the results of both quality responses were retrieved.

Step 8 (establish regression models). Secondly, the RSM is applied to establish the linear and nonlinear multivariate relationships between the design variables and the output responses. Because these relations were almost nonlinear, a full quadratic form was a suitable model for the CRPS as follows:

$$F_j = \beta_0 + \sum_{i=1}^{n} \beta_i x_i + \sum_{i=1}^{n} \beta_{ij} x^2{}_i + \sum_{i=1}^{n-1} \sum_{j=i+1}^{n} \beta_{ij} x_i x_j + \varepsilon_i \quad (6)$$

where the β_i (i=0, 1, 2, . . ., n) are unknown regression coffi-cients, β_{ij} $(i < j)$ are interaction coefficients, $x_1, x_2, \ldots, x_n$ are a set of n predictors believed to be related to a response F jth, and ε is a random error.

These objective functions were used for the TLBO algorithm.

Phase 3 (optimization using TLBO). Based on the objective functions which were determined in Step 8, the optimization process was implemented by TLBO algorithm. TLBO has been widely used [28–31] but it has been applied for the proposed stage. Operation principle of this algorithm imitates the teaching-learning ability of the teacher and learners in a classroom. The expected learning outcome of TLBO was the grades results of students which depended on the ability of teacher. It forecasted that a high quality student is the result of good training given by a good teacher. Moreover, besides learning from the teacher, the students can learn other knowledge from different classmates to improve their grades. Courses were considered design variables and the student's results were similar to the fitness value of the optimization process. The algorithm includes two phases: (i) teacher phase where candidates were randomly distributed over the search space and the best solution was defined and (ii) leaner phase where solutions tried to get new knowledge from interacting with other students.

Phase 4 (determine weight factor). In this paper, a high safety factor and a large displacement were expected. Hence, the signal to noise (S/N) ratio for both responses was calculated as

$$\eta = -10 \log \left(\frac{1}{q} \sum_{i=1}^{q} \frac{1}{f_i^2} \right), \quad (7)$$

where f_i denotes the quality response ith, e the experiment number, and q the number of replicates of experiment ith.

In this work, a large displacement is conflicted with a high safety factor. Generally, the trial-error method is used to find satisfaction between them but it needs a lot of time and cost and depends on the expert experience. To overcome the struggles, another alternative is to convert the multiple objectives into a single objective by multiplying each objective with a corresponding weight factor (WF) [38]. Commonly, the WF is determined based on the priority, expert experience, the direct assignment method, an eigenvector method, an empty method, a minimal information method, and a random determination and customer's demands but an optimal solution is very sensitive and of varying weight factor. If the WF should be calculated accurately and the optimal safety factor, output displacement could be exactly retrieved accordingly. Therefore, we followed the methods of Dao et al. [39] to calculate the WF for each response. In this study, based on the well-established mathematical equations, the WF was assigned for the safety factor and output displacement, respectively.

There were two objective functions in this paper; the sum weighted objective function was expressed by

$$f = w_1 f_1 + w_2 f_2, \tag{8}$$

where f_1, f_2 and f are safety factor, displacement, and sum weighted objective function, respectively. w_1, and w_2 indicated the weight values of f_1 and f_2, respectively. Therein, $0 \le w_i \le 1$ and $\sum_{i=1}^{2} w_i = 1$. The sum of weight is assumed to be a convex combination of the objectives. Each single optimization goal can be determined by a single optimal solution on the Pareto front.

The proposed scheme for determining the WF used the normalized sensitivity of each parameter for different objectives. The advantage of this method was the easiness to calculate the weighting values and it allowed an accurate adjustment of the weight value so that the optimal solution confirmed to the design goals. The calculation principle of this proposed method was described as follows.

Based on the TM, the optimal level of design parameters is corresponding to the highest *S/N* ratio value. Alternatively, according to the response table of average *S/N* ratios, the optimized solution is defined. The mean deviation between the minimum *S/N* ratio and the maximum *S/N* ratio of each level is calculated, as shown in the response table. This deviation is considered a mean range (max-min) for each level of each parameter. If the deviation is higher, the effect grade of each level of each parameter on each objective becomes larger. In other respects, if the mean range (max-min) for a level of a parameter is equal to zero, we can summarize that the parameter is not associated with the response. Alternatively, if the objective does not vary when the level of the parameter is changed, this shows that there is no correlation between the parameter and the response. We can summarize that both the WF and the *S/N* ratio have the significantly important effects on the responses, whereas, when the WF or the *S/N* ratio changes, the optimal solution is also varied.

So, the contribution grade of each parameter on each response can be regarded by the mean range (max-min) of *S/N* ratio. The mean range can be inspected as a quantity value of the contribution grade for each objective. Later on, the ratio of quantity value of each response is defined as a criterion in order to compute the WF. Because the unit of the safety factor and the output displacement (mm) is different, the mean *S/N* ratio of each level of each response has to be normalized as z_i ($0 \le z_i \le 1$)through the below so as to eliminate the influence of utilizing various units and decrease the difference. The aim of the normalization is to modify the values measured on various scales to a general scale. The normalized values of the mean *S/N* ratio change between 0 and 1.

The higher the better was utilized for both objectives; the normalized mean value of S/N ratios was normalized as follows:

$$z_i = \frac{\eta_i - \min \eta_i}{\max \eta_i - \min \eta_i}, \tag{9}$$

where z_i is the normalized mean *S/N* value for the ith response ($i = 1, 2, \ldots,$ n), n is the number of responses, and η_i illustrates the estimated *S/N* value from the TM. $\max \eta_i$ and $\min \eta_i$ are the largest and smallest values of η_i, respectively.

The mean range (max-min) of the normalized mean *S/N* ratio for each level of each parameter was computed as follows:

$$\begin{aligned} r_{ij} = {} & \max \left\{ z_{i,j,1}, z_{i,j,2}, \ldots, z_{i,j,r} \right\} \\ & - \min \left\{ z_{i,j,1}, z_{i,j,2}, \ldots, z_{i,j,r} \right\}, \end{aligned} \tag{10}$$

where r_{ij} is the mean range (max-min) of the normalized mean *S/N* ratio for each level of each design parameter $j = 1, 2, \ldots, q$, q is the number of design parameters, $r = 1, 2, \ldots, l$, l is the number of experimental level of each objective, and $z_{i,j,r}$ is the normalized mean value of *S/N* for the ith response of the parameter jth at the kth experiment.

The WF was computed by the following equation:

$$w_i = \frac{\sum_{j=1}^{q} r_{ij}}{\sum_{i=1}^{n} \sum_{j=1}^{q} r_{ij}}, \tag{11}$$

where w_i is the weight factor of ith objective and $w_i \ge 0$.

The sum weight factors for total objectives have to be equal to one:

$$\sum_{i=1}^{n} w_i = 1. \tag{12}$$

Phase 5 (statistical analysis for the proposed hybrid algorithm). In order to evaluate the behavior of the proposed hybrid algorithm, the Wilcoxon's rank signed test, which was a nonparametric statistical analysis, was applied. For details about this technique, the readers can refer to [40, 41]. A comparison of evolutionary algorithms was aimed to discover the significant difference between them with the hybrid algorithm.

Table 5: Process parameters and their levels (unit: mm).

Factors	Range	Level 1	Level 2	Level 3
A	51-53	51	52	53
B	1-1.2	1	1.1	1.2
C	0.5-0.7	0.5	0.6	0.7
D	0.5-0.7	0.5	0.6	0.7

Table 6: Experimental results and responses.

No.	A	B	C	D	Safety factor	Displacement (mm)
1	51	1	0.5	0.5	1.5800	2.1726
2	51	1.1	0.6	0.6	1.5645	1.8280
3	51	1.2	0.7	0.7	1.5348	1.6166
4	52	1	0.6	0.7	1.5587	1.7421
5	52	1.1	0.7	0.5	1.4766	1.6637
6	52	1.2	0.5	0.6	1.5866	2.0411
7	53	1	0.7	0.6	1.4634	1.5807
8	53	1.1	0.5	0.7	1.4821	1.9220
9	53	1.2	0.6	0.5	1.5091	1.9174

6. Results and Discussion

6.1. Collection of Data and Regression Models. Each factor was divided into three levels depending on specialized knowledge and designer experience, as illustrated in Table 5. The L_9 (3^4) orthogonal array of TM was used to establish the number of experiments. The safety factor (F_1) and displacement (F_2) were collected, as shown in Table 6.

Later on, the ANOVA was applied to determine the significant contribution of each parameter on the responses. Based on the data in Table 6, the MINITAB 18 software was used to analyze the experimental data.

The regression equations were gained as follows:

$$F_1 = -43.54 + 1.867A - 6.780B + 2.532C + 1.770D - 0.01832A * A + 3.103B * B - 2.352C * C - 1.462D * D \quad (13)$$

$$F_2 = 29.39 - 0.437A - 2.03B - 47.92C - 0.419D - 0.019A * B + 0.757AC + 5.856B * C \quad (14)$$

Tables 7 and 8 show the ANOVA results of the safety factor and displacement. This analysis was carried out at 5% significance level and 95% confidence level. In Table 7, it was observed that the contribution proportion on the safety factor F_1 of A and C and interaction between B and B were more significant than other design parameters with 47.44%, 28.42%, and 10.86%, respectively. In contrast, its proportion on the F_1 of B and D, interaction between C and C, interaction between A and A, and interaction between D and D were very small with 0.76%, 0.09%, 6.24%, 3.78%, and 2.41%, respectively. Therefore, to increase the safety factor, A and C should be significantly controlled. Moreover, as given in Table 8, the proportion on the displacement F_2 of C was highest with 84.34%, and its proportion of D was significantly higher at 11.61%. Meanwhile, the other effect factors listed had a much smaller contribution proportion. Its proportion of A and B as well as interaction between A and B, interaction between A and C, and interaction between B and C were 2.02%, 0.33%, 0.11%, 0.31%, and 1.25%, respectively. As a result, in order to raise the value of F_2, parameters C and D should be significantly controlled. Besides, the contribution percent of error was 0% and 0.03% for F_1 and F_2, respectively.

6.2. Sensitivity Analysis. Statistical technique was used to identify the effect degree of variables on the quality responses. As seen in Figure 9, factor A showed that, in the range from 51 mm to 52 mm, this parameter caused a slight reduction to F_1 and F_2, but, in the range from 52 mm to 53 m, it caused a sharp reduction to F_1 and a slight increase to F_2. In addition, factor B indicated that, in the range from 1 mm to 1.1 mm, it affected a dramatical decrease to F_1 and caused a slight increase to F_2; however, from 1.1 mm to 1.2 mm, there was a sharp increase to F_1 and a gradual rise to F_2.

As plottled in Figure 10, factor C revealed that, in the range from 0.5 mm to 0.6 mm, it affected a gradual decrease to F_1 and caused a sharp decrease to F_2, but, from 0.6 mm to 0.7 mm, there was a sharp increase to both F_1 and F_2. Finally, factor D showed that, in the range from 0.5 mm to 0.6 mm, it affected gradual increase to F_1 and caused a slight increase to F_2; however, from 0.6 mm to 0.7 mm, there was a gradual decrease to both F_1 and F_2.

In summary, overall effects of design variables were illustrated, as in Figure 11. It gives an increase and decrease range in each factor. From that, the designers could control the factors so as to achieve the best design for the proposed CRPS.

Based on the numerical results from Table 6, the S/N ratio values (η_1 and η_2) were computed by Eq. (9), as given in Table 9. And, then, the mean values and mean range for the normalized S/N ratios were computed for each level

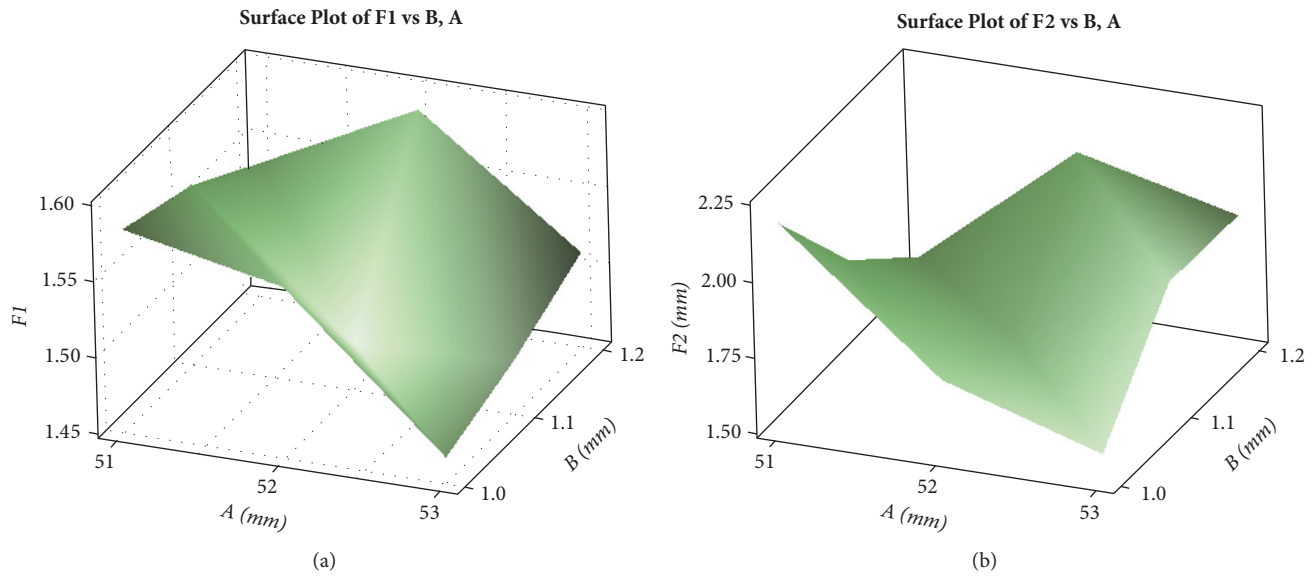

Figure 9: Effect diagram of A and B on (a) safety factor and (b) the output displacement.

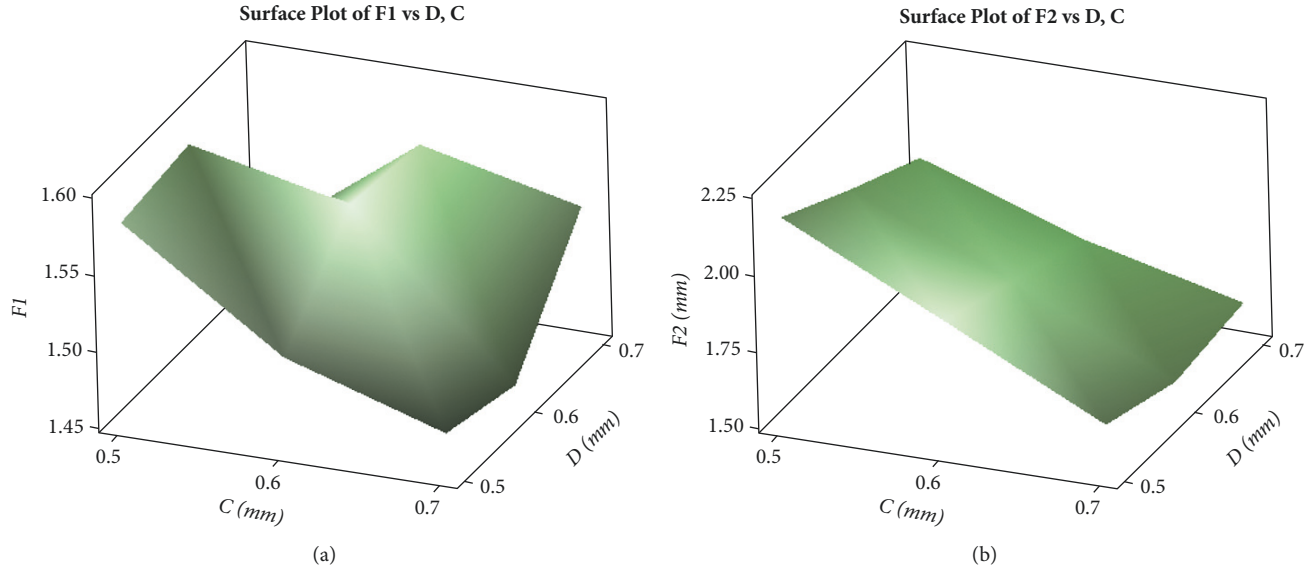

Figure 10: Effect diagram of C and D on (a) safety factor and (b) the output displacement.

of each parameter by using Eq. (10) and the results were illustrated in Table 10. Utilizing Eq. (11), the weight factor of each response was computed. As shown in Tables 11 and 12, the results indicated that the weight factors for safety factor and displacement are 0.5995 (59.95%) and 0.4005 (40.05%), respectively. These values were accurately determined based on the set of established equations, and then they were assigned for the further optimization process in the TLBO. Therefore, it illustrates that the displacement had a significant grade higher than that of the safety factor for the rotary stage. This was in agreement with the author's specialized knowledge and design experiences in the compliant mechanism area.

6.3. Optimal Results and Statistical Analysis. First of all, the number of numerical experiments was laid out using the TM. Next, a 3D FEM model was built and the numerical data were retrieved. Based on this data, the RSM was applied to establish the mathematical equations for the displacement and safety factor. And then, the WFs were determined using Equations (9)-(12). Based on the well-established Equations (13) and (14), the multiobjective optimization problem was solved through the TLBO approach. The optimization process was implemented using MATLAB 2017 software. The optimal results were found at A = 51 mm, B = 1 mm, C = 0.5 mm, D = 0.6674 mm, F_1 = 1.558, and F_2 = 2.096 mm. The results revealed that the optimal displacement satisfied the initial

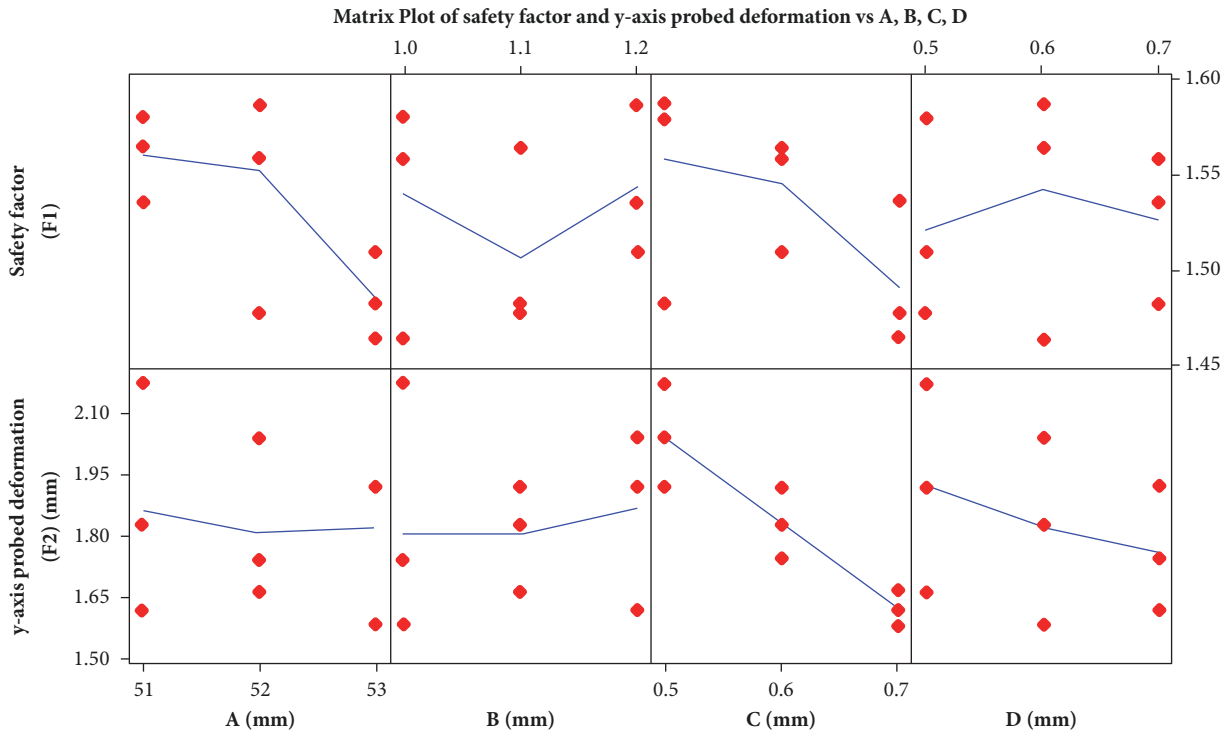

Figure 11: Sensitivity diagram of the controllable parameters on the responses.

Table 7: Analysis of variance for F_1.

Source	DF	Seq SS	Contribution	Adj SS	Adj MS	P-Value
Model	8	0.017736	100.00%	0.017736	0.002217	Significant
Linear	4	0.013606	76.71%	0.013606	0.003401	Significant
A	1	0.008415	47.44%	0.008415	0.008415	Significant
B	1	0.000134	0.76%	0.000134	0.000134	Significant
C	1	0.005040	28.42%	0.005040	0.005040	Significant
D	1	0.000016	0.09%	0.000016	0.000016	Significant
Square	4	0.004130	23.29%	0.004130	0.001033	Significant
A∗*A*	1	0.000671	3.78%	0.000671	0.000671	Significant
B∗*B*	1	0.001926	10.86%	0.001926	0.001926	Significant
C∗*C*	1	0.001106	6.24%	0.001106	0.001106	Significant
D∗*D*	1	0.000427	2.41%	0.000427	0.000427	Significant
Error	0					
Total	8	0.017736	100.00%			

requirements and is suitable for the nanoindentation tester system. In addition, the results found that the safety factor is a relatively good value so as to guarantee a long working efficiency and long fatigue life.

The next step is that the effectiveness of the proposed algorithm was compared with other evolutionary algorithms such as adaptive elitist differential evolution (AEDE) algorithm [9]. The optimal parameters were utilized to build a 3D model for simulation validation in ANSYS software 18.2 in order to evaluate the error between the FEM and the proposed hybrid approach. The process was conducted with the same constraints and the same input displacement.

In order to evaluate the statistic behavior of the hybrid optimization algorithm, a statistical analysis was used in this study. The Wilcoxon's rank signed test was applied to describe the behavior of the proposed algorithm. The computational simulations were conducted, 40 runs for each algorithm. The Wilcoxon's rank signed test was performed at 5% significant level and 95% confidence intervals. The results of Wilcoxon's rank signed test were given in Tables 13 and 14.

As is known, a null hypothesis assumed that there is no significant difference between mean values of the two algorithms. As given in Tables 13 and 14, the results show that the p-value is less than 0.05 (5% significance level) which

Table 8: Analysis of variance for F_2.

Source	DF	Seq SS	Contribution	Adj SS	Adj MS	P-Value
Model	7	0.320994	99.97%	0.320994	0.045856	0.036
Linear	4	0.315632	98.30%	0.120716	0.030179	0.043
A	1	0.006475	2.02%	0.000033	0.000033	0.667
B	1	0.001059	0.33%	0.004390	0.004390	0.096
C	1	0.270810	84.34%	0.076496	0.076496	0.023
D	1	0.037288	11.61%	0.001507	0.001507	0.161
2-Way Interaction	3	0.005362	1.67%	0.005362	0.001787	0.172
$A*B$	1	0.000355	0.11%	0.000002	0.000002	0.910
$A*C$	1	0.001007	0.31%	0.003340	0.003340	0.109
$B*C$	1	0.004000	1.25%	0.004000	0.004000	0.100
Error	1	0.000101	0.03%	0.000101	0.000101	
Total	8	0.321094	100.00%			

Table 9: The experimental results and S/N ratios.

Trial No.	f_1	f_2 (mm)	η_1 of f_1 (dB)	η_2 of f_2 (dB)
1	1.5800	2.1726	3.9731	6.7396
2	1.5645	1.8280	3.8875	5.2395
3	1.5348	1.6166	3.7210	4.1721
4	1.5587	1.7421	3.8553	4.8215
5	1.4766	1.6637	3.3853	4.4215
6	1.5866	2.0411	4.0093	6.1973
7	1.4634	1.5807	3.3073	3.9770
8	1.4821	1.9220	3.4176	5.6751
9	1.5091	1.9174	3.5744	5.6543

Table 10: The values of normalized S/N ratios (z_i).

S/N ratios		Normalized S/N ratios (z_i)	
η_1 (dB)	η_2 (dB)	z_1 of η_1	z_2 of η_2
3.9731	6.7396	0.9484	1.0000
3.8875	5.2395	0.8265	0.4570
3.7210	4.1721	0.5893	0.0706
3.8553	4.8215	0.7805	0.3057
3.3853	4.4215	0.1111	0.1609
4.0093	6.1973	1.0000	0.8037
3.3073	3.9770	0.0000	0.0000
3.4176	5.6751	0.1571	0.6147
3.5744	5.6543	0.3804	0.6071

Table 11: The weight factor for the safety factor.

Level	The mean value of normalized S/N ratios at each level			
	A	B	C	D
Level 1	0.7881	0.5764	0.7019	0.4800
Level 2	0.6306	0.3649	0.6625	0.6088
Level 3	0.1792	0.6566	0.2858	0.5090
Range r_{ij}	0.6089	0.2917	0.4160	0.1288
Weight factor for the safety factor: w_1 = 0.5995				

Table 12: The weight factor for the displacement.

Level	The mean value of normalized S/N ratios at each level			
	A	B	C	D
Level 1	0.5092	0.4352	0.8036	0.5893
Level 2	0.4234	0.4109	0.4202	0.4202
Level 3	0.4073	0.4938	0.2821	0.3303
Range r_{ij}	0.1019	0.0830	0.5215	0.2590
Weight factor for the displacement: w_2 = 0.4005				

Table 13: Wilcoxon's comparison of proposed algorithm vs AEDE for the safety factor.

Number for tests	Estimated median	p-value	Wilcoxon statistic
40	0.0020	0.000	820

Table 14: Wilcoxon's comparison of proposed algorithm vs AEDE for the displacement.

Sample for test	Estimated median	p-value	Wilcoxon statistic
40	0.00175	0.000	820

is a strong evidence against the null hypothesis. It means that there is a statistical difference between the proposed algorithm and AEDE algorithm. It shows that the proposed hybrid algorithm is better than the AEDE algorithm in solving the multiobjective optimization design in this paper.

Another way, the Friedman test [42] was the nonparametric approach, being alternative to the one-way ANOVA with repeated measures. This approach would determine the difference between the proposed hybrid optimization approach and the AEDE algorithm at significant level of α = 0.05. The Friedman test for the safety factor and displacement was conducted, separately. The computational simulations were conducted, 40 runs for each algorithm. The results showed that the p-value is less than 0.05. As a result, the null hypothesis was rejected. It could be concluded that there is a difference between the proposed hybrid optimization approach and the AEDE, as given in Tables 15 and 16.

7. Validation

The optimal parameters (A = 51 mm, B = 1 mm, C = 0.5 mm, D = 0.6674 mm, F_1 = 1.558, and F_2 = 2.096 mm) were used to build a 3D model for simulation validation. The process was performed with the same constraints and the same input displacement. FEA model result was established from the predicted result of the hybrid approach. The maximum of deformation was about 2.096 mm and the minimum of safety factor was approximately 1.558. Table 17 illustrates that the error between predicted results and validations for the displacement and safety factor are 6.82% and 0.3%, respectively. It means that the predicted solutions are in good agreement with the validated results.

Compared with the initial design, the optimal results were better than the initial ones. An improvement after optimizing for the safety factor was about 3.708% and for the displacement was approximately 18.498%, as given in Table 18. It shows that the proposed hybrid algorithm is an efficient approach to multiobjective optimization design of the CRPS.

8. Conclusions

This paper presented an efficient hybrid optimization algorithm for the compliant rotary positioning stage for nanoindentation tester. The CRPS imitated the biomechanical behavior of beetle animal in order to reach a linear displacement and more flexibility. To enhance the working stroke and safety factor, the geometric parameters of the proposed CRPS were optimized via a hybrid algorithm of the TM, FEM, RSM, and TLBO. The weight factors of displacement and safety factor were calculated by establishing the sets of equations.

The result found that the WFs of safety factor and displacement are 0.5995 (59.95%) and 0.4005 (40.05%), respectively. These WF's values were assigned into the TLBO algorithm to solve the multiobjective optimization problem. The sensitivity analysis and ANOVA were carried out to determine the effects and significant contributions of design variables to the quality responses. The results indicated that the optimal parameters were found at A = 51 mm, B = 1 mm, C = 0.5 mm, and D = 0.6674 mm. Moreover, the results indicated that the optimal safety factor is 1.558 and the optimal displacement is approximately 2.096 mm. It showed that the predicted results are in good agreement with the validations. Based on the Wilcoxon's rank signed test and Friedman test, the proposed hybrid optimization algorithm was better than the AEDE algorithm. The hybrid optimization is an efficient approach to solve the multiobjective optimization problem for complex design.

Data Availability

The authors state that the data used to support the findings of this study are included within the article.

Table 15: Friedman test for the safety factor.

Response	Number of tests	Median	Sum of Ranks
Safety factor by proposed method	40	1.5586	80.0
Safety factor by AEDE	40	1.5566	40.0
Overall	80	1.5576	
DF	Chi-Square	P-Value	
1	40.00	0.000	
Null hypothesis		H_0: All treatment effects are zero	
Alternative hypothesis		H_1: Not all treatment effects are zero	

Table 16: Friedman test for the displacement.

Response	Number of tests	Median	Sum of Ranks
Safety factor by proposed method	40	2.096	80.0
Safety factor by AEDE	40	2.094	40.0
Overall	80	2.095	
DF	Chi-Square	P-Value	
1	40.00	0.000	
Null hypothesis		H_0: All treatment effects are zero	
Alternative hypothesis		H_1: Not all treatment effects are zero	

Table 17: Error between predicted result and validations.

Responses	Prediction	Validation	Error (%)
F_1	1.558	1.5533	0.30
F_2 (mm)	2.096	1.9621	6.82

Table 18: Improvement between initial design and optimal design.

Performances	Initial design	Optimal design	Improvement (%)
F_1	1.5023	1.558	3.708
F_2 (mm)	1.7688	2.096	18.498

Conflicts of Interest

The authors declare that there are no conflicts of interest regarding the publication of this article.

Acknowledgments

The authors are thankful for the financial support from the HCMC University of Technology and Education, Vietnam, under Grant No. T2019-06TĐ.

References

[1] Z. Hu, K. J. Lynne, S. P. Markondapatnaikuni, and F. Delfanian, "Material elastic-plastic property characterization by nanoindentation testing coupled with computer modeling," *Materials Science and Engineering: A Structural Materials: Properties, Microstructure and Processing*, vol. 587, pp. 268–282, 2013.

[2] J. Nohava, N. X. Randall, and N. Conté, "Novel ultra nanoindentation method with extremely low thermal drift: Principle and experimental results," *Journal of Materials Research*, vol. 24, no. 3, pp. 873–882, 2009.

[3] W. O'Brien, "Long-range motion with nanometer precision," *Photonics Spectra*, vol. 39, no. 6, pp. 80-81, 2005.

[4] L.-J. Lai and Z.-N. Zhu, "Design, modeling and testing of a novel flexure-based displacement amplification mechanism," *Sensors and Actuators A: Physical*, vol. 266, pp. 122–129, 2017.

[5] S. Polit and J. Dong, "Development of a high-bandwidth XY nanopositioning stage for high-rate micro-/nanomanufacturing," *IEEE/ASME Transactions on Mechatronics*, vol. 16, no. 4, pp. 724–733, 2011.

[6] M.-G. Song, H.-W. Baek, N.-C. Park et al., "Development of small sized actuator with compliant mechanism for optical image stabilization," *IEEE Transactions on Magnetics*, vol. 46, no. 6, pp. 2369–2372, 2010.

[7] T.-P. Dao and S.-C. Huang, "Compliant thin-walled joint based on zygoptera nonlinear geometry," *Journal of Mechanical Science and Technology*, vol. 31, no. 3, pp. 1293–1303, 2017.

[8] R. F. Fung, Y. L. Hsu, and M. S. Huang, "System identification of a dual-stage XY precision positioning table," *Precision Engineering*, vol. 33, no. 1, pp. 71–80, 2009.

[9] T.-P. Dao, N. L. Ho, T. T. Nguyen et al., "Analysis and optimization of a micro-displacement sensor for compliant micrograpper," *Microsystem Technologies*, vol. 23, no. 12, pp. 5375–5395, 2017.

[10] T.-P. Dao and S.-C. Huang, "Design and multi-objective optimization for a broad self-amplified 2-DOF monolithic mechanism," *Sādhanā*, vol. 42, no. 9, pp. 1527–1542, 2017.

[11] W.-L. Zhu, Z. Zhu, P. Guo, and B.-F. Ju, "A novel hybrid actuation mechanism based XY nanopositioning stage with totally decoupled kinematics," *Mechanical Systems and Signal Processing*, vol. 99, pp. 747–759, 2018.

[12] H. Kim, D. Ahn, and D. Gweon, "Development of a novel 3-degrees of freedom flexure based positioning system," *Review of Scientific Instruments*, vol. 83, no. 5, p. 055114, 2012.

[13] Q. Xu, "Design of a large-range compliant rotary micropositioning stage with angle and torque sensing," *IEEE Sensors Journal*, vol. 15, no. 4, pp. 2419–2430, 2015.

[14] Q. Xu, "Design and testing of a novel multi-stroke micropositioning system with variable resolutions," *Review of Scientific Instruments*, vol. 85, no. 2, p. 025002, 2014.

[15] P. Wang and Q. Xu, "Design of a flexure-based constant-force XY precision positioning stage," *Mechanism and Machine Theory*, vol. 108, pp. 1–13, 2017.

[16] H. Wang and X. Zhang, "Input coupling analysis and optimal design of a 3-DOF compliant micro-positioning stage," *Mechanism and Machine Theory*, vol. 43, no. 4, pp. 400–410, 2008.

[17] S.-C. Huang and T.-P. Dao, "Design and computational optimization of a flexure-based XY positioning platform using FEA-based response surface methodology," *International Journal of Precision Engineering and Manufacturing*, vol. 17, no. 8, pp. 1035–1048, 2016.

[18] N. L. Chau, T. Dao, and V. T. Nguyen, "Optimal Design of a Dragonfly-Inspired Compliant Joint for Camera Positioning System of Nanoindentation Tester Based on a Hybrid Integration of Jaya-ANFIS," *Mathematical Problems in Engineering*, vol. 2018, Article ID 8546095, 16 pages, 2018.

[19] N. L. Ho, T. Dao, H. G. Le, and N. L. Chau, "Optimal Design of a Compliant Micrograpper for Assemble System of Cell Phone Vibration Motor Using a Hybrid Approach of ANFIS and Jaya," *Arabian Journal for Science and Engineering*, pp. 1–16, 2018.

[20] N. Le Chau, V. A. Dang, H. G. Le, and T.-P. Dao, "Robust Parameter Design and Analysis of a Leaf Compliant Joint for Micropositioning Systems," *Arabian Journal for Science and Engineering*, vol. 42, no. 11, pp. 4811–4823, 2017.

[21] A. Konak, D. W. Coit, and A. E. Smith, "Multi-objective optimization using genetic algorithms: a tutorial," *Reliability Engineering & System Safety*, vol. 91, no. 9, pp. 992–1007, 2006.

[22] G. Jones, P. Willett, R. C. Glen, A. R. Leach, and R. Taylor, "Development and validation of a genetic algorithm for flexible docking," *Journal of Molecular Biology*, vol. 267, no. 3, pp. 727–748, 1997.

[23] C. Andrés and S. Lozano, "A particle swarm optimization algorithm for part–machine grouping," *Robotics and Computer-Integrated Manufacturing*, vol. 22, no. 5-6, pp. 468–474, 2006.

[24] M. J. Esfandiari, G. S. Urgessa, S. Sheikholarefin, and S. H. Dehghan Manshadi, "Optimization of reinforced concrete frames subjected to historical time-history loadings using DMPSO algorithm," *Structural and Multidisciplinary Optimization*, vol. 58, no. 5, pp. 2119–2134, 2018.

[25] M. Esfandiari, G. Urgessa, S. Sheikholarefin, and S. D. Manshadi, "Optimum design of 3D reinforced concrete frames using DMPSO algorithm," *Advances in Engineering Software*, vol. 115, pp. 149–160, 2018.

[26] P. K. Das, H. S. Behera, and B. K. Panigrahi, "A hybridization of an improved particle swarm optimization and gravitational search algorithm for multi-robot path planning," *Swarm and Evolutionary Computation*, vol. 28, pp. 14–28, 2016.

[27] A. K. Qin, V. L. Huang, and P. N. Suganthan, "Differential evolution algorithm with strategy adaptation for global numerical optimization," *IEEE Transactions on Evolutionary Computation*, vol. 13, no. 2, pp. 398–417, 2009.

[28] R. V. Rao and V. Patel, "Multi-objective optimization of heat exchangers using a modified teaching-learning-based optimization algorithm," *Applied Mathematical Modelling*, vol. 37, no. 3, pp. 1147–1162, 2013.

[29] R. V. Rao, V. J. Savsani, and D. P. Vakharia, "Teaching-learning-based optimization: a novel method for constrained mechanical design optimization problems," *Computer-Aided Design*, vol. 43, no. 3, pp. 303–315, 2011.

[30] R. V. Rao, V. J. Savsani, and D. P. Vakharia, "Teaching-learning-based optimization: an optimization method for continuous non-linear large scale problems," *Information Sciences*, vol. 183, no. 1, pp. 1–15, 2012.

[31] R. V. Rao, *Teaching Learning Based Optimization and Its Engineering Applications*, Springer International Publishing Switzerland, Basel, Switzerland, 2016.

[32] T. H. Hou, C. H. Su, and W. L. Liu, "Parameters optimization of a nano-particle wet milling process using the Taguchi method, response surface method and genetic algorithm," *Powder Technology*, vol. 173, no. 3, pp. 153–162, 2007.

[33] T.-P. Dao, S.-C. Huang, and P. T. Thang, "Hybrid Taguchi-cuckoo search algorithm for optimization of a compliant focus positioning platform," *Applied Soft Computing*, vol. 57, pp. 526–538, 2017.

[34] E. Burman, D. Elfverson, P. Hansbo, M. G. Larson, and K. Larsson, "Shape optimization using the cut finite element method," *Computer Methods Applied Mechanics and Engineering*, vol. 328, pp. 242–261, 2018.

[35] A. Albanesi, F. Bre, V. Fachinotti, and C. Gebhardt, "Simultaneous ply-order, ply-number and ply-drop optimization of laminate wind turbine blades using the inverse finite element method," *Composite Structures*, vol. 184, pp. 894–903, 2018.

[36] A. Karamanlı and T. P. Vo, "Size dependent bending analysis of two directional functionally graded microbeams via a quasi-3D theory and finite element method," *Composites Part B: Engineering*, vol. 144, pp. 171–183, 2018.

[37] S.-C. Huang and T.-P. Dao, "Multi-objective optimal design of a 2-DOF flexure-based mechanism using hybrid approach of Grey-Taguchi coupled response surface methodology and entropy measurement," *Arabian Journal for Science and Engineering*, vol. 41, no. 12, pp. 5215–5231, 2016.

[38] W. Stadler, "A survey of multicriteria optimization or the vector maximum problem, Part I. 1776–1960," *Journal of Optimization Theory and Applications*, vol. 29, no. 1, pp. 1–52, 1979.

[39] T.-P. Dao, S.-C. Huang, and N. Le Chau, "Robust parameter design for a compliant micrograpper based on hybrid Taguchi-differential evolution algorithm," *Microsystem Technologies*, vol. 24, no. 3, pp. 1461–1477, 2018.

[40] E. Cuevas, J. Gálvez, S. Hinojosa, O. Avalos, D. Zaldívar, and M. Pérez-Cisneros, "A comparison of evolutionary computation techniques for IIR model identification," *Journal of Applied Mathematics*, vol. 2014, Article ID 827206, 9 pages, 2014.

[41] S. García, D. Molina, M. Lozano, and F. Herrera, "A study on the use of non-parametric tests for analyzing the evolutionary algorithms' behaviour: a case study on the CEC'2005 Special Session on Real Parameter Optimization," *Journal of Heuristics*, vol. 15, no. 6, pp. 617–644, 2009.

[42] M. Friedman, "A comparison of alternative tests of significance for the problem of m rankings," *The Annals of Mathematical Statistics*, vol. 11, no. 1, pp. 86–92, 1940.